Electron Transfer in a Virtual Quantum State of $LiBH_4$ Induced by Strong Optical Fields and Mapped by Femtosecond X-Ray Diffraction

J. Stingl,[1] F. Zamponi,[1] B. Freyer,[1] M. Woerner,[1] T. Elsaesser,[1] and A. Borgschulte[2]

[1]*Max-Born-Institut für Nichtlineare Optik und Kurzzeitspektroskopie, 12489 Berlin, Germany*

[2]*EMPA, Swiss Federal Laboratories for Materials Testing and Research, Laboratory for Hydrogen and Energy, CH-8600 Dübendorf, Switzerland*

(Received 9 May 2012; published 2 October 2012)

Transient polarizations connected with a spatial redistribution of electronic charge in a mixed quantum state are induced by optical fields of high amplitude. We determine for the first time the related transient electron density maps, applying femtosecond x-ray powder diffraction as a structure probe. The prototype ionic material $LiBH_4$ driven nonresonantly by an intense sub-40 fs optical pulse displays a large-amplitude fully reversible electron transfer from the BH_4^- anion to the Li^+ cation during excitation. Our results establish this mechanism as the source of the strong optical polarization which agrees quantitatively with theoretical estimates.

DOI: 10.1103/PhysRevLett.109.147402 PACS numbers: 78.47.J−, 72.20.Ht, 78.70.Ck

The interaction of condensed matter with strong optical fields induces a spatial relocation of electrons, connected with a time-dependent electric polarization. This mechanism is at the heart of nonlinear optics both with isolated atoms in the gas phase [1] and in condensed phases [2]. It also plays a key role for nonequilibrium charge transport in solids [3]. While the optical and/or electrical responses have been studied in detail for a large variety of systems, the underlying charge relocations in space have remained unknown in most cases. To determine the latter in a quantitative way, structure probes such as x-ray diffraction in the ultrafast time domain are required [4–8].

A judicious choice of the crystalline material is required for elucidating charge relocations by ultrafast x-ray diffraction. First, to bring out the motion of valence electrons, the number of core electrons that contribute to the x-ray diffraction signal should be small; i.e., light atoms or ions are preferred. Second, the electric polarizability of the material should be high and, third, the band gap E_{gap} between the highest valence and the lowest conduction band should be large to allow for nonresonant interactions with optical pulses. Such conditions are matched by the ionic crystal $LiBH_4$ which has been studied in some detail and received substantial interest as a high energy density and hydrogen storage material [9]. The BH_4^- anion has a very high electric polarizability, $\alpha_e = 7.2 \times 10^{-40}\ \mathrm{C\,m^2\,V^{-1}}$ [10] which is 40 times larger than that of the hydrogen atom. The large $E_{\mathrm{gap}} \approx 7$ eV allows for nonresonant interactions with femtosecond pulses at near-infrared wavelengths. Electron density and band structure calculations show that mainly orbitals on the B and H atoms contribute to the highest valence band while states in the lowest conduction band involve orbitals of the B and Li atoms [11,12].

A basic microscopic mechanism that should be essential for the material's polarization induced by a strong external field is illustrated in Fig. 1, showing a schematic of the ionic potentials of Li^+ and BH_4^- together with a valence band (VB) and a conduction band (CB) state. Without external field, valence electrons are in the highest VB state with a wave function $|\Psi_{\mathrm{VB}}\rangle$ displaying a much higher amplitude on the BH_4^- than on the Li^+ site. An external field of an amplitude comparable to the interionic field of the order of 10^9 V/m distorts the ionic potentials and leads to the admixture of other ionic states, in particular conduction band states $|\Psi_{\mathrm{CB}}\rangle$ with a similar amplitude on the two sites. In other words, the strong external field generates a mixed state with a wave function $|\Psi_{\mathrm{virt}}\rangle = \alpha|\Psi_{\mathrm{CB}}\rangle + \beta|\Psi_{\mathrm{VB}}\rangle$ [13]. This mixed state is characterized by a net shift of electronic charge from the BH_4^- to the Li^+ site over the large interionic distance. This results in a strong electric polarization of the material existing as long as the external field is present. In this Letter, we provide the first direct evidence for this mechanism by deriving quantitative transient electron density maps from a femtosecond x-ray diffraction pattern.

At $T = 300$ K, $LiBH_4$ crystallizes in the orthorhombic space group Pnma (No. 62). The unit cell dimensions are $a = 0.718$ nm, $b = 0.444$ nm, $c = 0.680$ nm [14] with four formula units per unit cell [Fig. 3(b)]. The sample studied in our experiments (95% purity Alfa Aesar and Katchem) was carefully pulverized (crystallites of roughly 1 μm diameter), pressed at 0.9 Gpa, and then put in the sample holder. Because of the high chemical reactivity, great care was taken to avoid air contamination of the sample which was prepared under an Ar atmosphere in a glovebox. The ≈ 600 μm thick powder sample was kept in a small cell sealed with diamond windows (thickness 20 μm). During the measurements, the sample was continuously rotated.

The experiment was performed in an optical pump/x-ray probe scheme [7,15]. Femtosecond pulses from an amplified Ti:sapphire laser system (1 kHz repetition rate,

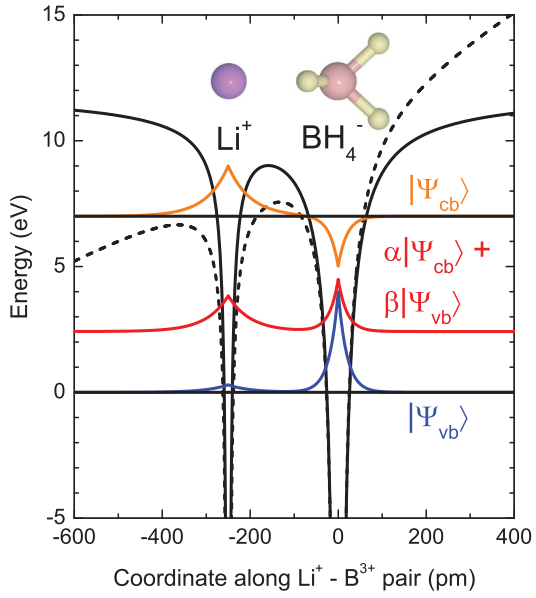

FIG. 1 (color). Schematic illustrating the mechanism of electron transfer from a BH_4^- to a Li^+ ion in a $LiBH_4$ crystal. The unperturbed valence and conduction band wave functions, Ψ_{VB} and Ψ_{CB} (blue and orange curves), and the ionic potentials (solid black lines) are plotted as a function of the interionic distance. In the valence band, electrons are mainly localized on the BH_4^+ ion while the conduction band wave function displays similar amplitudes on the two ions. Upon application of an external electric field with an amplitude comparable to the interionic fields, the potentials are distorted (dashed black line) and the corresponding perturbed wave function $\alpha\Psi_{VB} + \beta\Psi_{CB}$ (red line) is a mixture of valence and conduction band states of the unperturbed Hamiltonian. Generation of this mixed state is connected with a partial electron transfer from the BH_4^- to the Li^+ ion and a strong electric polarization. In time, the electron transfer follows the external electric field.

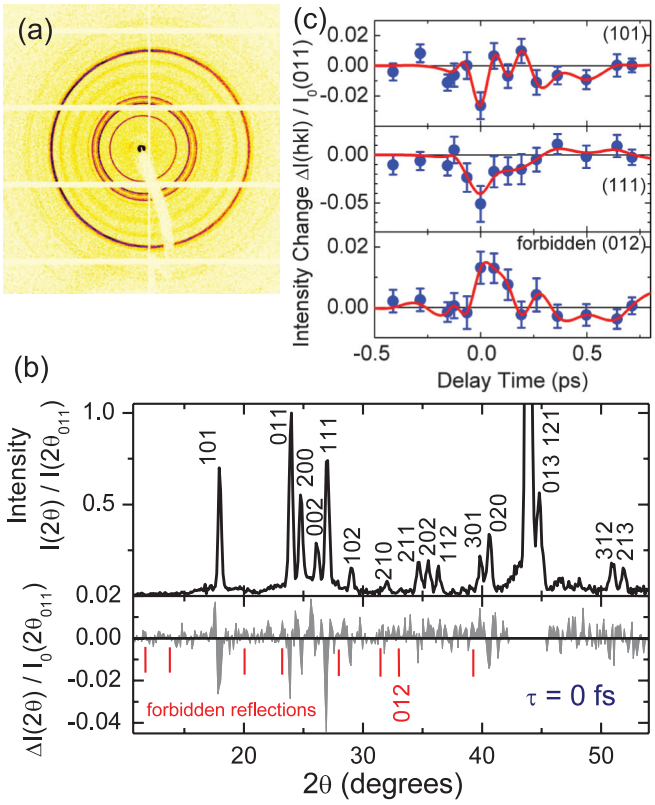

FIG. 2 (color). (a) X-ray powder diffraction pattern of $LiBH_4$ acquired on a large-area detector (integration time 140 s). (b) Upper panel: x-ray intensity integrated over individual diffraction rings as a function of the diffraction angle 2θ. The numbers indicate the set of lattice planes. The very strong reflection at $2\theta = 44$ degree originates from the diamond windows of the sample. Lower panel: Intensity changes of the diffraction peaks measured at zero delay between the excitation pulse and the x-ray probe pulses as a function of 2θ. The intensity change $\Delta I(2\theta)$ is normalized to the steady state intensity I_0 of the 011 peak. In addition to the allowed reflections, a number of forbidden reflections (marked by red lines) occur, due to a change of the crystal symmetry upon excitation. (c) Transient intensity changes for three selected reflections as a function of pump-probe delay (symbols). The red lines are a guide to the eye.

5 mJ per pulse, 35 fs pulse duration, 800 nm central wavelength) were divided by a beam splitter and 5 percent of the laser output served as sub-40 fs excitation pulses with a peak intensity of about 4×10^{11} W/cm^2 on the sample, corresponding to a maximum field amplitude of 1.6×10^9 V/m. The main part of the laser output was used to generate synchronized 100-fs hard x-ray pulses in a Cu $K\alpha$ plasma source (wavelength 0.154 nm) which has been described in detail elsewhere [16]. The x-ray diffraction pattern, consisting of Debye-Scherrer diffraction rings, was recorded with a large-area detector (Dectris Pilatus 1M). A series of such patterns measured at different delay times after excitation allowed for reconstructing the momentary charge distributions. The time delay zero between pump and probe pulses was determined before and after each series of x-ray measurements. This procedure allowed for safely merging data sets recorded on different days of measurement. The optical excitation with pulses around $E = 1.5$ eV $\ll E_{gap} \approx 7$ eV was strongly nonresonant [11,12]. Multiphoton excitation of the material can be ruled out as is evident from the absence of any time-integrating long-term signal in the pump-probe transients.

A powder pattern acquired without excitation and an integration time of 140 s is shown in Fig. 2(a). In Fig. 2(b) (upper panel), the intensity integrated over individual diffraction rings is plotted as a function of the diffraction angle 2θ. The assignment of the different peaks to particular sets of lattice planes was derived from a comparison with literature data [14]. Upon interaction with the pump pulse, the ring pattern displays intensity changes of up to 4×10^{-2} [lower panel of Fig. 2(b)]. While the angular positions of the allowed reflections remain unchanged within the experimental accuracy of 0.1 degrees, there are a number of new reflections (marked by red lines)

which are forbidden in the equilibrium geometry of the unit cell. Their occurrence points to a transient symmetry breaking of the equilibrium geometry in presence of the strong field of the excitation pulse. Figure 2(c) shows the time evolution of the changes of diffracted intensity on 3 different reflections, the allowed (101) and (111) rings as well as the forbidden (012) ring. For each delay time, the x-ray intensity was integrated over approximately 10^5 s. The transients display an essentially pulse limited intensity change around delay zero, followed by very small intensity changes at longer delay times.

The transient changes of diffracted x-ray intensity $\Delta I_{hkl}(t)/I^0_{011}$ are related to structure factors for a particular set hkl of lattice planes:

$$\frac{\Delta I_{hkl}(t)}{I^0_{011}} \propto \frac{|F_{hkl}(t)|^2 - |F^0_{hkl}|^2}{|F^0_{011}|^2}, \quad (1)$$

where $F_{hkl}(t)$ is the structure factor of the material modified by the external electric field and F^0_{hkl} the known structure factor of the unexcited crystal (I^0_{011}: steady state intensity of the 011 reflection). The structure factors are complex quantities described by an amplitude and a phase. The (time dependent) electron density $\rho(\mathbf{r}, t)$ is given by the Fourier transform of the structure factors. The equilibrium charge density $\rho_0(\mathbf{r})$ was derived from the known structure and structure factors of the unexcited crystal. To derive the transient $\rho(\mathbf{r}, t)$ from the measured transient diffraction patterns [8], the complex phase factors need to be known. In the present case, the occurrence of forbidden reflections with an unknown phase of the structure factor represents an additional complication. Here, we use a procedure which combines the so-called maximum entropy method with a Patterson function approach to derive the transient charge densities [17–22].

Since we are measuring a powder sample, the electric field vector of the pump laser $\mathbf{E}(t)$ has in each crystallite an individual orientation relative to its crystal axes. The transient change of the electron density in an individual crystallite i, $\Delta\rho_i(\mathbf{r}, t) = \rho_i(\mathbf{r}, t) - \rho_0(\mathbf{r})$ can be decomposed into symmetry conserving and a nonconserving component $\Delta\rho_i(\mathbf{r}, t) = \Delta\rho^{\mathrm{Sym}}(\mathbf{r}, |\mathbf{E}(t)|) + \Delta\rho_i^{\mathrm{NoSym}}(\mathbf{r}, \mathbf{E}(t))$. The symmetry conserving part depends only on the amplitude of the electric field $|\mathbf{E}(t)|$ and, thus, is identical in all crystallites. Since the distribution of relative orientations between $\mathbf{E}(t)$ and crystal axes is isotropic in a powder sample, the symmetry conserving electron density change is just the electron density change averaged over all crystallites: $\Delta\rho_{\mathrm{Sym}}(\mathbf{r}, t) = N^{-1}\sum_{i=1}^{N}\Delta\rho_i(\mathbf{r}, t)$. In this averaging procedure, the symmetry nonconserving components cancel each other since for each crystallite a with $\Delta\rho_a^{\mathrm{NoSym}}(\mathbf{r}, \mathbf{E}(t))$ one will find within the ensemble another crystallite b with $\Delta\rho_b^{\mathrm{NoSym}}(\mathbf{r}, \mathbf{E}(t)) = -\Delta\rho_a^{\mathrm{NoSym}}(\mathbf{r}, \mathbf{E}(t))$. As a consequence, $\Delta\rho_{\mathrm{Sym}}(\mathbf{r}, t)$ exhibits the symmetry properties of the initial structure $\rho_0(\mathbf{r})$ and we can use the maximum entropy method [23] to reconstruct $\Delta\rho_{\mathrm{Sym}}(\mathbf{r}, t)$. Please note that $\Delta\rho_{\mathrm{Sym}}(\mathbf{r}, t)$ is exclusively determined by the intensity changes of the *allowed* reflections.

To assess the relevance of symmetry changes of the electron density which result in the occurrence of forbidden reflections, we performed model calculations based on the Patterson method [17]. The quantity $\rho(\mathbf{r})$ is the Fourier transform of F_{hkl}, whereas the Patterson function $\mathrm{Patt}(\mathbf{r})$ is given by the Fourier transform of $|F_{hkl}|^2$. The Patterson function is equivalent to the spatial autocorrelation of the electron density distribution $\mathrm{Patt}(\mathbf{r}) = \int \rho(\mathbf{r}')\rho(\mathbf{r} + \mathbf{r}')d^3\mathbf{r}'$. The drawbacks of the use of $\mathrm{Patt}(\mathbf{r})$ are the increased number of peaks [for N atoms in the unit cell, $\mathrm{Patt}(\mathbf{r})$ has $N(N-1)$ correlation peaks] and peak broadening. With our spatial resolution, the overlap becomes a serious problem and hinders the direct application of this technique to our data set.

Nevertheless, the relevance of symmetry breaking and the relative weight of $\Delta\rho^{\mathrm{Sym}}(\mathbf{r}, |\mathbf{E}(t)|)$ vs $\Delta\rho_i^{\mathrm{NoSym}}(\mathbf{r}, \mathbf{E}(t))$ can be estimated with the help of the Patterson method. We calculated the transient changes of two different 3D-Patterson functions $\Delta\mathrm{Patt}(\mathbf{r} = 0, t) = \mathrm{Patt}(\mathbf{r} = 0, t) - \mathrm{Patt}_0(\mathbf{r} = 0)$ at the origin which were derived from the transient $|F_{hkl}(t)|^2$ values of (i) only allowed and (ii) allowed + forbidden reflections. Both curves (not shown) exhibit a pronounced decrease of $\Delta\mathrm{Patt}(\mathbf{r} = 0, t)$ around delay zero due to the charge transfer. The difference between data including all reflections and the data including the allowed reflections only is within the experimental uncertainty at all delay times. We conclude that the contribution $\Delta\rho_i^{\mathrm{NoSym}}(\mathbf{r}, \mathbf{E}(t))$ is much smaller than $\Delta\rho^{\mathrm{Sym}}(\mathbf{r}, |\mathbf{E}(t)|)$ within individual crystallites and, thus, the quantity $\Delta\rho_{\mathrm{Sym}}(\mathbf{r}, t)$ gives a realistic picture of the change of electron density. Thus, the symmetry nonconserving component will be neglected in the following.

The unit cell of $LiBH_4^-$ is shown in Fig. 3(b). In Fig. 3(a), we plot the equilibrium electron density $\rho_0(\mathbf{r})$ in the crystal plane $Y = 0.25$ [see Fig. 3(b)] which contains a Li^+ and a BH_4^- ion. This map shows a high electron density on the BH_4^- ion and a small density on the Li^+ ion (cf., cartoon of the conduction band wave function in Fig. 1). In Fig. 3(c), the change of electron density $\Delta\rho(\mathbf{r}, t) = \Delta\rho_{\mathrm{Sym}}(\mathbf{r}, t)$ is plotted for zero delay time. This map shows a pronounced decrease of electron density on the BH_4^- unit and a corresponding increase on the Li^+ ion, giving direct evidence for a transfer of electronic charge between these ions and a concomitant electric polarization. The x-ray diffraction pattern and, thus, the charge density map averages over all manifestations of the charge transfer in the powder sample which contains crystallites of random orientation relative to the electric field direction of the excitation pulse. Each BH_4^- ion has four nearest Li^+ neighbors which are not distinguished in the diffraction pattern and, thus, contribute with the same weight to the average charge density map. As a consequence, the charge transfer mechanism can be

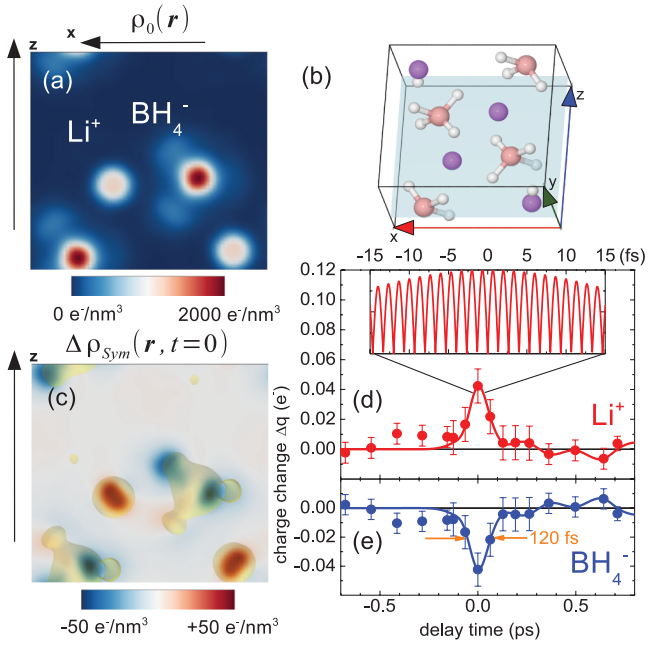

FIG. 3 (color). (a) Stationary total electron density distribution in the plane $Y = 0.25$ [see (b)], convoluted in the reciprocal space with a Gaussian to fit our spatial resolution. (b) Unit cell of $LiBH_4$: Li atoms are violet, H white, and B pink. The $Y = 0.25$ plane is shown in transparent light blue. (c) Change of electron density $\Delta\rho_{\mathrm{Sym}}$ in the $Y = 0.25$ plane at zero delay between the optical excitation and the x-ray probe pulses. Note the different scales of the color bars. The isosurface of the stationary electron density distribution is shown in yellow. (d), (e) Amount of transferred charge Δq integrated over the subvolumes of the Li^+ and BH_4^- ions as a function of pump-probe delay. The transients show sharp spikes of Δq around delay zero with about 120 fs full width at half maximum, the width of the temporal correlation of excitation and probe pulses. The solid lines are a guide to the eye. The inset in (d) shows the calculated time dependence of the modulus of the polarization.

adequately discussed by summarizing this geometry in a single "effective" Li^+/BH_4^- ion pair.

To determine the amount of charge transferred, we divided the unit cell into subvolumes each containing one atom, by assigning each spatial position $\mathbf{r}$ within the unit cell uniquely to the subvolume of the nearest atom defined by the nuclear positions of the initial structure. We then integrated the charge in the subvolumes. In the case of BH_4^-, the charge of the whole unit was put together. Time-dependent charge density changes are displayed in Figs. 3(d) and 3(e). The striking feature is a sharp drop of electronic charge on the BH_4^- unit [Fig. 3(e)] concomitant with the increase of the same amplitude on the Li^+ ions [Fig. 3(d)] around pump-probe delay zero. The peaks around delay zero have a width of approximately 120 fs (FWHM) which agrees with the temporal cross-correlation function of the optical excitation and the hard x-ray probe pulses [7]. For the following 700 fs, there are minor changes of electron density. Such facts strongly support our picture of a field-driven charge transfer which is limited in time to the presence of the driving field. Changes in the sign of the 800 nm driving field of a 2.66 fs period lead to a local charge transfer in a different pair of BH_4^- and Li^+ ions which is oriented in the opposite spatial direction and makes an identical contribution to the transient charge density map. As a result, the modulus of the macroscopic polarization oscillates as sketched in the inset of Fig. 3(d). From the amount of transferred charge of $0.04e$ (e: elementary electron charge) and the distance between the Li^+ and BH_4^- ions, one estimates a high transient polarization $P/e = 1.0 \times 10^{-11}$ m per effective ion pair.

We now compare the measured polarization amplitude with the polarization estimated from the polarizability of the BH_4^- ion and the applied electric field of the excitation pulse of 1.6×10^9 V/m. BH_4^- anion in vacuum was calculated to be $\alpha_e = 7.2 \times 10^{-40}$ C m^2 V^{-1} [10]. In the solid state, the polarizability can be estimated from the refractive index of the material via the Clausius-Mossotti relation. There are no reliable refractive index data for $LiBH_4$ crystals in the literature as larger crystals of this material are very difficult to grow. However, from a comparison of the measured values of its isomorphs (refractive index $n = 1.547$, 1.490, 1.487, 1.498 for $NaBH_4$, KBH_4, $RbBH_4$, and $CsBH_4$, respectively) [24], one estimates a value of $n = 1.6$ at 800 nm which corresponds to a polarizability of $\alpha_e \approx 1.9 \times 10^{-39}$ C m^2 V^{-1}, substantially larger than the calculated polarizability of the isolated anion. By plugging in the electric field of the excitation pulse, one estimates a transient polarization of the crystal of $P/e = 1.8 \times 10^{-11}$ m per ion pair. This value is in very good agreement with the polarization derived above from the amount of transferred electron charge and the spatial separation of the Li^+ and BH_4^- ions. Such agreement shows that the charge transfer between the two ions represents the major source term of the electric polarization generated in the high optical field.

In conclusion, we have directly observed a fully reversible charge transfer between neighboring Li^+ and BH_4^- ions in $LiBH_4$, driven by the high electric field of an ultrashort optical pulse. This transfer results in a strong electric polarization which is limited in time to the femtosecond duration of the driving pulse. The "instantaneous" character of the electronic response suggests applications for characterizing the temporal structure of hard x-ray pulses by cross-correlating them with ultrashort optical pulses. The polarization amplitude derived from the transient electron density map and the spatial separation of the Li^+ and BH_4^- ions is in good agreement with the value estimated from the BH_4^- polarizability at optical frequencies. Our results represent a direct measurement of the electron density in a mixed quantum state generated by a strong external field. The methodology applied here paves

the way for studying the microscopic nature of virtual states in a broad range of light-matter interactions under strong-field conditions.

This research has received funding from the European Research Council under the European Union's Seventh Framework Programme (FP7/2007-2012)/ERC Grant Agreement 247051 and from the Deutsche Forschungsgemeinschaft (Grant No. WO 558/13-1).

[1] P. Eckle, A. N. Pfeiffer, C. Cirelli, A. Staudte, R. Dörner, H. G. Muller, M. Büttiker, and U. Keller, Science **322**, 1525 (2008).
[2] N. Bloembergen, Science **216**, 1057 (1982).
[3] W. Kuehn, P. Gaal, K. Reimann, M. Woerner, T. Elsaesser, and R. Hey, Phys. Rev. Lett. **104**, 146 602 (2010).
[4] M. Bargheer, N. Zhavoronkov, Y. Gritsai, J. C. Woo, D. S. Kim, M. Woerner, and T. Elsaesser, Science **306**, 1771 (2004).
[5] M. Braun, C. v. Korff-Schmising, M. Kiel, N. Zhavoronkov, J. Dreyer, M. Bargheer, T. Elsaesser, C. Root, T. E. Schrader, P. Gilch, W. Zinth, and M. Woerner, Phys. Rev. Lett. **98**, 248301 (2007).
[6] D. M. Fritz *et al.*, Science **315**, 633 (2007).
[7] M. Woerner, F. Zamponi, Z. Ansari, J. Dreyer, B. Freyer, M. Prémont-Schwarz, and T. Elsaesser, J. Chem. Phys. **133**, 064509 (2010).
[8] F. Zamponi, P. Rothhardt, J. Stingl, M. Woerner, and T. Elsaesser, Proc. Natl. Acad. Sci. U.S.A. **109**, 5207 (2012).
[9] A. Züttel, A. Borgschulte, and S.-I. Orimo, Scr. Mater. **56**, 823 (2007).
[10] E. L. Albasiny and J. R. A. Cooper, Proc. Phys. Soc. London **82**, 801 (1963).
[11] Q. Ge, J. Phys. Chem. A **108**, 8682 (2004).
[12] K. Miwa, N. Ohba, S. Towata, Y. Nakamori, and S. Orimo, Phys. Rev. B **69**, 245 120 (2004).
[13] C. Cohen-Tannoudji, B. Diu, and F. Laloë, *Quantum Mechanics* (Wiley, New York, 1977), Vol. 1–2.
[14] J. Soulié, G. Renaudin, R. Cerny, and K. Yvon, J. Alloys Compd. **346**, 200 (2002).
[15] F. Zamponi, Z. Ansari, M. Woerner, and T. Elsaesser, Opt. Express **18**, 947 (2010).
[16] N. Zhavoronkov, Y. Gritsai, M. Bargheer, M. Woerner, Th. Elsaesser, F. Zamponi, I. Uschmann, and E. Förster, Opt. Lett. **30**, 1737 (2005).
[17] A. L. Patterson, Phys. Rev. **46**, 372 (1934).
[18] E. T. Jaynes, Phys. Rev. **106**, 620 (1957).
[19] C. J. Gilmore, Acta Crystallogr. Sect. A **52**, 561 (1996).
[20] S. van Smaalen, L. Palatinus, and M. Schneider, Acta Crystallogr. Sect. A **59**, 459 (2003).
[21] R. Y. de Vries, W. J. Briels, and D. Feil, Phys. Rev. Lett. **77**, 1719 (1996).
[22] L. Palatinus and S. van Smaalen, Acta Crystallogr. Sect. A **61**, 363 (2005).
[23] In our data analysis we used the maximum entropy method (MEM) [18,19] as implemented in the BayMEM software [20].
[24] M. D. Banus, R. W. Bragdon, and A. A. Hinckley, J. Am. Chem. Soc. **76**, 3848 (1954).